Method for patient-specific finite element modeling and simulation of deep brain stimulation

Mattias Åström, Ludvic U Zrinzo, Stephen Tisch, Elina Tripoliti,
Marwan I Hariz and Karin Wårdell

Method for patient-specific finite element modelling and simulation of deep brain stimulation

Mattias Åström[1], Ludvic U. Zrinzo[2], Stephen Tisch[2], Elina Tripoliti[2], Marwan I. Hariz[2,3] and Karin Wårdell[1]

[1]*Department of Biomedical Engineering, Linköping University, Sweden*

[2]*Institute of Neurology, Queen Square, University College London, UK*

[3]*Department of Neurosurgery, University Hospital, Umeå, Sweden*

Corresponding author

Mattias Åström

Department of Biomedical Engineering

Linköping University

581 85 Linköping, Sweden

E-mail: matas@imt.liu.se

Phone: +46 (0) 736 290978

Fax: +46 (0)13 101902

Abstract Deep brain stimulation (DBS) is an established treatment for Parkinson's disease (PD). Success of DBS is highly dependent on electrode location and electrical parameter settings. The aim of this study was to develop a general method for setting up patient-specific 3D computer models of DBS, based on magnetic resonance images, and to demonstrate the use of such models for assessing the position of the electrode contacts and the distribution of the electric field in relation to individual patient anatomy. A software tool was developed for creating finite element DBS-models. The electric field generated by DBS was simulated in one patient and the result was visualized with isolevels and glyphs. The result was evaluated and corresponded well with reported effects and side effects of stimulation. It was demonstrated that patient-specific finite element models and simulations of DBS can be useful for increasing the understanding of the clinical outcome of DBS.

Keywords Deep brain stimulation, patient-specific, simulation, finite element, glyph.

1. Introduction

Deep brain stimulation (DBS) is an established surgical treatment for movement disorders which can be highly effective in reducing the motor symptoms of idiopathic Parkinson's disease (PD) that are refractory to medical management [1]. Common DBS targets for PD are the subthalamic nucleus (STN), the globus pallidus internus (GPi) and the ventralis intermedius nucleus (Vim) of the thalamus. Although no large controlled clinical trials comparing the different targets has yet been published, DBS in STN seems to give the most consistent alleviation of the majority of PD symptoms, and is at present the most common surgical therapy [2-6]. However, STN DBS is sometimes accompanied by postoperative adverse effects such as decrease in verbal fluency, depression and hypomania [7]. Thus, the success of STN DBS for PD patients is highly dependent on patient selection and subsequent accuracy in target determination as well as stimulation parameters settings. Precise knowledge of the anatomical location of an electrode contact in brain target nuclei is a crucial step in understanding the expected effects and side effects of stimulation. However, of equal importance is knowledge of the anatomical extent of the electric field surrounding the active electrode contact. Models and simulations are one method for exploring the clinical outcome of DBS.

The distribution of the electric potential in the vicinity of a DBS electrode has previously been modelled using isotropic homogenous tissue [8-16]. More recently, Butson et al. [17] presented a three dimensional (3D) patient-specific method to predict the volume of tissue activated by DBS based on diffusion tensor images (DTI). However, the spatial resolution of DTI is still rather poor and DTI is not an available technique in many clinical centres. The overall aim of the present study was to develop a general method for setting up patient-specific 3D finite element models of DBS based on pre- and postoperative magnetic

resonance images (MRI) acquired during DBS surgery. A secondary aim was to demonstrate the use of such models for assessing the position of the active electrode contacts and the spatial distribution of the electric field in relation to individual patient anatomy.

2. Materials and Methods

2.1 Patient-specific DBS model

A patient-specific heterogeneous finite element computer model of DBS in the subthalamic nucleus was set up. The DBS model was based on axial T2 weighted stereotactic MRI of a PD patient undergoing DBS implantation. Preoperative stereotactic MRI was used for setting up a model of the brain, and postoperative stereotactic MRI for positioning the DBS electrodes at their true position in the brain. The Leksell Stereotactic System® (Elekta Instrument AB, Sweden) was utilized during the surgery and both the pre- and postoperative images were acquired on a 1.5 Tesla scanner (GE Signa, General Electric Medical Systems, WI, USA) with an MRI voxel volume of 0.98x0.98x2.0 mm without slice separation. However, the picture archiving and communication system (PACS) (Agfa, UK) altered the voxel volume of the MRI to 0.49x0.49x2.0 mm by interpolation. The model was based on the interpolated images. The size of the brain model was limited to 60x40x40 mm (214,389 voxels) covering the bilateral STN and the surrounding structures.

2.1.1. Brain model

A software tool was developed in MatLab 7.0 (The MathWorks Inc., USA) to set up an anatomical property matrix for the finite element brain model. The property matrix was based on preoperative MRI voxel intensity data which were classified into different tissues. Intensity based segmentation was used to identify anatomical areas with grey matter, white matter, cerebrospinal fluid and large blood vessels in several different MR-images. An average intensity value was calculated for each tissue respectively. The presence of iron in part of the STN lowered the intensity data values in this structure, which appeared hypointense in the T2 weighted MRI [18]. Therefore, an additional average intensity value was calculated for grey matter containing iron. The classified MRI voxels were allotted electrical conductivity

properties from the literature. A random neuronal orientation was assumed, thus isotropic electrical conductivity values at a frequency of 145 Hz from Andreuccetti's online database [19] was used (table 1). Particular voxels may contain more than one tissue, giving rise to partial volume effects. Thus, a linear step function was used to allot approximated electrical physical properties to such voxels. The material properties were mapped in the finite element model at coordinates corresponding to their original location in the MRI data set. The result was a matrix of electrical brain properties with the same resolution as the MRI data set (figure 1).

2.1.2. Electrode positions

Two DBS electrodes (Model 3389 DBS™ Lead, Medtronic, Inc. USA) with a radius of 0.635 mm and contact lengths of 1.5 mm separated by 0.5 mm, were modelled and positioned in the brain model. The electrode contacts were indexed from 0 to 7, starting at the left, most ventral electrode contact (figure 2 a). In order to position the electrodes at their true positions in the model, a second finite element brain model based on the postoperative MRI was set up, where the electrode models were positioned in the centre of the electrode artefacts.

A software tool for registration of the pre- and postoperative stereotactic MRI data sets was developed in MatLab 7.0. The registration was performed by selecting stereotactic markers in the pre- and postoperative images. A transformation matrix describing the transformation from the postoperative to the preoperative coordinate system was then calculated (figure 2b). The transformation matrix was applied to the electrodes in the postoperative model which were transferred to the preoperative brain model.

2.1.3 DBS parameter settings

Two weeks after the patient underwent implantation of the DBS system (Medtronic Kinetra® neurostimulation system), the clinical effects of various electrical DBS settings were assessed

by a neurologist experienced in the treatment of PD with DBS. The clinically most effective electrical parameter settings were used as input for the simulation (table 2). In correspondence with these settings, bilateral monopolar electrode configuration was set up, where electrode contacts 1 (left) and 7 (right) were active and set to -4.0 V and -3.5 V respectively. However, in a study by Butson and McIntyre [20], it was shown that the stimulation waveforms produced by Medtronic's implantable pulse generators (Kinetra® and Soletra®) differed from their theoretical waveforms. Thus, the electric potential settings were normalized to -3.5 V (left) and -3.0 V (right) according to the voltage threshold correction factors (0.87 and 0.87) of their study (table 2). The electrical conductivity of the electrode contacts were approximated to $15*10^6$ S/m (a mix of platinum and iridium) and the outer boundaries of the brain anatomy were used as anode (ground) to mimic a monopolar electrode configuration.

2.2. Mesh density and governing equation

The finite element brain model was set up in a multiphysic modelling program (Comsol Multiphysics 3.2, Comsol AB, Sweden). The domains, including the brain model anatomy and the electrode models, were divided into ~2,000,000 tetrahedral mesh elements with the highest mesh density close to the electrodes. In order to retain the spatial resolution of the MRI, the maximum element length was set to 1 mm.

The electrical conductivity properties at the integration points were calculated by linear interpolation of the mapped electrical conductivity values. The equation for steady currents was used to calculate the electric potential distribution in the vicinity of the electrodes [21]:

$$\nabla \cdot J = -\nabla \cdot [\sigma \nabla V] = 0 \ (\mathrm{A\ m^{-3}}) \qquad (1)$$

where J is the current density (A m^{-2}), σ the electrical conductivity (S m^{-1}), and V the electric potential (V). The model was solved on a 64-bit Linux computer (3.6 GHz Intel Xeon

processor, 16 GB RAM) for ~ 2,500,000 number of degrees of freedom using Comsol Multiphysics' iterative linear system solver *GMRES* with the preconditioner *Incomplete LU*.

2.3. Evaluation of electrode positions

A surgical planning system, the FrameLink Planning Station™ (Medtronic, Minneapolis, MN, USA) was used by an experienced user as a reference system in order to evaluate the accuracy of the position of the modelled electrode positions. The positions of the artefacts from the most ventral and dorsal, left and right electrode contacts (electrode contacts 0, 3, 4 and 7) were marked in the postoperative MRI and transferred to the preoperative MRI using the FrameLink Planning Station™. Images from the finite element model at the level of the electrode contacts were also rendered. The position of the electrodes in the finite element model was compared with the positions of the electrodes in the preoperative MRI by superimposing the images onto each other.

2.4. Visualization

During patient-specific modelling and simulation of DBS, various electrical entities may be visualized. In this study the electric potential, the electric field, and the second difference of the electric potential were visualized in 3D. The electric field, which is the gradient of the electric potential, describes the rate of change of the electric potential. In order to identify the anatomical aspect of the electric field, the mapped material properties in the model were replaced with the MRI intensity data after the model was solved. This made it possible to visualize the MRI intensity data on colour-coded slices together with the distribution of the electric field. During standard DBS settings it has been suggested that the outer boundary of the volume of influence may roughly be estimated to a 2 to 5 mm radius from the electrode contact [22]. In this study, the electric field isolevel 0.2 V/mm, which lies within this range, was chosen. This isolevel has earlier been suggested by Hemm et al. [12] in a model based

study with homogenous tissue to fit with the lateral GPi borders during one case of GPi stimulation.

In order to illustrate the impact of the electric field on a straight axon (depolarisation and hyperpolarisation), the second order difference of the electric potential can be visualized [23]. McNeal showed in 1976 that the rate of change of the transmembrane voltage at each node of Ranvier was determined by the second order difference of the electric potential at each node. The second order difference of the electric potential was later named the activating function by Rattay [24]. In order to visualize the activating function for all directions in 3D, a software tool was developed in MatLab 7.0 for calculation of second order tensor fields. A common way to visualize all degrees of freedom of second order tensors is to use glyphs, where each tensor is represented with a geometric object [25, 26]. Two elliptic glyphs were rendered in every sampled point; one black glyph for visualization of depolarisation of a straight axon, and one white glyph for visualization of hyperpolarisation of a straight axon. The eigenvectors were used as the principal axes, and the eigenvalues the radii of the ellipsoids. The activating function tensor D, was calculated for each point according to:

$$D = \begin{bmatrix} D_{xx} & D_{xy} & D_{xz} \\ D_{yx} & D_{yy} & D_{yz} \\ D_{zx} & D_{zy} & D_{zz} \end{bmatrix} \qquad (2)$$

The electric potential data used for the calculation of the activating function in the axial plane was sampled at 7x7=49 points with a sampling distance of 2 by 2 mm. Due to the rapid increase of the activating function close to the active electrode contact, the size of the ellipsoids closest to the active contact had to be capped and are not displayed in their full size.

3. Results

A patient-specific finite element model of the brain, based on pre- and postoperative MRI, was set up and the electric potential generated by the DBS electrodes during clinically effective parameter settings was simulated. The electric potential, the electric field, and the activating function were visualized in 3D (figure 3a-c, e-f). An axial MRI was also visualized for comparison of the spatial resolution of the model anatomy with the MRI (figure 3d). The position of the active electrode contacts in relation to the anatomy could clearly be identified in the model. It was shown that the left electrode contact was positioned slightly more dorsal and medial than the right electrode. During the clinically effective parameter settings, the electric field generated by the left electrode was located more ventral and medial in the anatomy than the electric field generated by the right electrode. It was also shown that the simulated isolevel volume was slightly larger in the vicinity of the left electrode than in the vicinity of the right electrode. This was in agreement with the higher amplitude (electrical potential) settings of the left electrode contact than of the right electrode contact (-3.5 V and -3.0 V respectively). The electric potential, the electric field, and the activating function was also visualized in one dimension, along a straight axon positioned in the vicinity of the left electrode (figure 4).

The accuracy of the position of the modelled electrodes was evaluated with a surgical planning system, the FrameLink Planning Station^{TM} (Medtronic, Minneapolis, MN, USA). The maximum difference between the position of the modelled electrode contacts and the marked electrode contacts in the preoperative MRI was less than 0.6 mm in all three dimensions (figure 5).

4. Discussion

A general method for creating patient-specific finite element models and simulations of DBS, based on MRI, was presented. It was shown that model-based investigations utilizing patient-specific finite element models of DBS can be used for visualizing the electric field and the position of the electrode contacts in relation to the anatomy. A method for visualizing the activating function in 3D in the vicinity of the active electrode contacts was also presented. A second order tensor field was calculated and two elliptic glyphs, describing depolarisation and hyperpolarisation of straight axons, were rendered in every sample point. The use of tensor fields to describe the activating function may be useful for setting up realistic DBS models of the basal ganglia, where activating of multiple neuron orientations are assessed simultaneously. Since the activating function is valid in one dimension and the visualized 0.2 V/mm electric field isolevel is valid in three dimensions, there is no direct relationship between the two. Thus, the activating function and the electric field are two central entities that should be used for different visualization purposes.

The clinically effective DBS settings reduced the major motor symptoms of the disease (tremor, akinesia and rigidity) initially without side effects except some euphoria and disinhibition. However, some 8 weeks post implantation the motor improvement decreased and the patient developed severe dysarthria and dysphonia as well as a degree of hypomania. In a study by Plaha et al. [27] stimulation related dysarthria were seen in patients who had electrode contacts medially placed in the STN. The authors believed this was due to spread of current to the fasciculus cerebello-thalamicus. These suggestions are in agreement with our simulations were the 0.2 V/mm isolevel generated by both electrodes covered part of the fasciculus cerebello-thalamicus (figure 6 a). Ulla et al. [28] reported that one patient who had benefited from bilateral DBS in the STN for PD, presented acute and reproducible manic

behavior when stimulated mainly in the substantia nigra. In agreement with this study, our simulations showed that part of the substantia nigra pars reticulata was covered by the 0.2 V/mm isolevel generated by the left electrode (figure 6 b). The patient in this study was later re-operated due to the dysarthria, where the left electrode was moved posterolaterally in order to avoid stimulation of the fasciculus cerebello-thalamicus and the substantia nigra pars reticulata, and the right electrode was moved dorsally in order to avoid stimulation of the fasciculus cerebello-thalamicus.

Patient-specific models and simulations of DBS can be used in clinical practice to provide the neurologist and neurosurgeon with a visual reference of the active electrode contact location and the distribution of the electric field in the anatomy. This method may be used both preoperatively, when planning the surgical procedure, as well as postoperatively, when programming the DBS device. Patient-specific DBS models may be particularly useful for visualizing the electric field in patients with unusual anatomical variations in the brain e.g. cystic cavities, which could be the case when stimulating in the GPi [8, 29], or when new targets are tried such as the subgenual cingulate region (Brodmann area 25) targeted for 6 patients with refractory depression [30]. Patient-specific models and simulations may also be used within other research areas e.g. biochemical investigations with microdialysis, or simulation of thermal phenomenon during radio-frequency lesioning in the brain.

Despite the great potentials of patient-specific models and simulations, it is important to recognize that the presented method does not model all aspects of DBS in their full complexity. It is only the distribution of the electric field that has been simulated. The other DBS parameters, such as the frequency and pulse length which are highly influencing the DBS clinical effects, must be added when connecting these results to e.g. neuron models.

Most importantly, the 0.2 V/mm electric field isolevel should only be interpreted as a boundary of tissue where the electric field is 0.2 V/mm or larger, and not as the volume of tissue influenced by the stimulation. Various neural components (soma, axons, and dendrites) are affected differently depending on their size and orientation in the electric field, and the volume of tissue influenced by DBS is still not known. The classification of the different brain matters were performed manually by the use of voxel intensity based segmentation. A complicating factor of intensity based classification is the possibility that two different voxels with the same intensity in the MRI may not necessarily contain the same tissue. In addition, although the hypointensity of the STN in the T2 weighted MRI was compensated for during the classification process, the presence of iron in part of the STN may result in misclassification of the tissues. Another source of error may be the electrical conductivity values for grey and white matter, which is highly frequency dependent and varies in the literature [19, 31-33]. In a study by Hemm et al. [34] it has also been shown to be significant individual variations in the electrical conductivity of brain tissue. The anisotropy of white matter was not modelled. The anisotropy of white matter has earlier been accounted for in modelling studies with promising results by deriving electrical conductivity tensors from diffusion tensor images (DTI) [35]. However, the resolution of the DTI images that can be produced with 1.5 Tesla scanners is rather poor and the small anisotropic fibre paths in the vicinity of the electrode e.g. the fasciculus cerebello-thalamicus, fasciculus lenticularis etc will not be visible in such DTI. Nonetheless, the anisotropy of large fiber tracks such as capsula interna will be well represented in DTI. The capacitive components of the electrode-tissue interface were ignored and no morphological changes such as encapsulation and scar tissue, which generally form within a few weeks after implantation, were included in this model. At this point the simulations serve as a rough estimation of the distribution of the

electric field in the anatomy for which relative changes in e.g. stimulation settings or electrode contact position can be studied.

In conclusion, a general method for setting up patient-specific 3D finite element models of DBS was presented. The use of such models for assessing the position of the active electrode contacts and the spatial distribution of the electric field in relation to individual patient anatomy was demonstrated. The anatomical distribution of the simulated electric field could be related to the reported effects and side effects of stimulation. Patient-specific models and simulations may be used for both pre- and postoperative investigations in order to increase the understanding of the clinical outcome of DBS.

Acknowledgements This work was supported by the Swedish Foundation for Strategic Research (SSF), Swedish Research Council (VR) and Swedish Governmental Agency for Innovation Systems (VINNOVA). The authors would like to thank Johannes Johansson for valuable discussions, Johan Tervald for graphical advice, and Göran Salerud for valuable comments on the manuscript.

References

1. Benabid A L, Chabardes S, Seigneuret E et al (2006) Surgical therapy for Parkinson's disease. J Neural Transm Suppl, 70: 383-92.
2. Burchiel K J, Anderson V C, Favre J et al (1999) Comparison of pallidal and subthalamic nucleus deep brain stimulation for advanced Parkinson's disease: results of a randomized, blinded pilot study. Neurosurgery, 456: 1375-82; discussion 1382-4.
3. Kleiner-Fisman G, Herzog J, Fisman D N et al (2006) Subthalamic nucleus deep brain stimulation: summary and meta-analysis of outcomes. Mov Disord, 21 Suppl 14: S290-304.
4. Krack P, Pollak P, Limousin P et al (1998) Subthalamic nucleus or internal pallidal stimulation in young onset Parkinson's disease. Brain, 121 451-7.
5. Pollak P, Fraix V, Krack P et al (2002) Treatment results: Parkinson's disease. Mov Disord, 17 Suppl 3: S75-83.
6. Volkmann J (2004) Deep brain stimulation for the treatment of Parkinson's disease. J Clin Neurophysiol, 211: 6-17.
7. Lang A E, Houeto J L, Krack P et al (2006) Deep brain stimulation: preoperative issues. Mov Disord, 21 Suppl 14: S171-96.
8. Astrom M, Johansson J D, Hariz M I et al (2006) The effect of cystic cavities on deep brain stimulation in the basal ganglia: a simulation-based study. J Neural Eng, 32: 132-8.
9. Butson C R, Maks C B, and McIntyre C C (2006) Sources and effects of electrode impedance during deep brain stimulation. Clin Neurophysiol, 1172: 447-54.
10. Butson C R and McIntyre C C (2006) Role of electrode design on the volume of tissue activated during deep brain stimulation. J Neural Eng, 31: 1-8.
11. Gimsa U, Schreiber U, Habel B et al (2006) Matching geometry and stimulation parameters of electrodes for deep brain stimulation experiments--numerical considerations. J Neurosci Methods, 1502: 212-27.
12. Hemm S, Mennessier G, Vayssiere N et al (2005) Deep brain stimulation in movement disorders: stereotactic coregistration of two-dimensional electrical field modeling and magnetic resonance imaging. J Neurosurg, 1036: 949-55.
13. Kuncel A M and Grill W M (2004) Selection of stimulus parameters for deep brain stimulation. Clin Neurophysiol, 11511: 2431-41.
14. McIntyre C C, Grill W M, Sherman D L et al (2004) Cellular effects of deep brain stimulation: model-based analysis of activation and inhibition. J Neurophysiol, 914: 1457-69.
15. Wei X F and Grill W M (2005) Current density distributions, field distributions and impedance analysis of segmented deep brain stimulation electrodes. J Neural Eng, 24: 139-47.
16. Miocinovic S, Parent M, Butson C R et al (2006) Computational analysis of subthalamic nucleus and lenticular fasciculus activation during therapeutic deep brain stimulation. J Neurophysiol, 963: 1569-80.
17. Butson C R, Cooper S E, Henderson J M et al (2007) Patient-specific analysis of the volume of tissue activated during deep brain stimulation. Neuroimage, 342: 661-70.
18. Dormont D, Ricciardi K G, Tande D et al (2004) Is the subthalamic nucleus hypointense on T2-weighted images? A correlation study using MR imaging and stereotactic atlas data. AJNR Am J Neuroradiol, 259: 1516-23.
19. Andreuccetti D, Fossi R, and Petrucci C (2005) Dielectric properties of body tissue. Italian National Research Council, Institute for Applied Physics, Florence, Italy http://niremf.ifac.cnr.it/tissprop/
20. Butson C R and McIntyre C C (2007) Differences among implanted pulse generator waveforms cause variations in the neural response to deep brain stimulation. Clin Neurophysiol, 1188: 1889-94.
21. Cheng D K (1989) Field and Wave Electromagnetics. Vol. ISBN 0-201-52820-7. 1989: Addison-Wesley Publishing Company Inc.
22. Volkmann J, Moro E, and Pahwa R (2006) Basic algorithms for the programming of deep brain stimulation in Parkinson's disease. Mov Disord, 21 Suppl 14: S284-9.
23. Holsheimer J, *Principles of neurostimulation*, in *Electrical Stimulation and the Relief of Pain*, B.A. Simpson, Editor. 2003, Elsevier: Amsterdam, The Netherlands. p. 17-36.
24. Rattay F (1986) Analysis of models for external stimulation of axons. IEEE Trans Biomed Eng, 3310: 974-7.
25. Sigfridsson A, Ebbers T, Heiberg E et al (2002) Tensor field visualisation using adaptive filtering of noise fields combined with glyph rendering. Visualization, 1-1 371-378.
26. Wiklund J, Nicolas V, Alface P R et al, *T-flash: Tensor visualization in medical studio.*, in *In Similar NoE Tensor Workshop.* 2006: Las Palmas, Spain.

27. Plaha P, Ben-Shlomo Y, Patel N K et al (2006) Stimulation of the caudal zona incerta is superior to stimulation of the subthalamic nucleus in improving contralateral parkinsonism. Brain, 129Pt 7: 1732-47.
28. Ulla M, Thobois S, Lemaire J J et al (2006) Manic behaviour induced by deep-brain stimulation in Parkinson's disease: evidence of substantia nigra implication? J Neurol Neurosurg Psychiatry, 7712: 1363-6.
29. Laitinen L V, Chudy D, Tengvar M et al (2000) Dilated perivascular spaces in the putamen and pallidum in patients with Parkinson's disease scheduled for pallidotomy: a comparison between MRI findings and clinical symptoms and signs. Mov Disord, 156: 1139-44.
30. Mayberg H S, Lozano A M, Voon V et al (2005) Deep brain stimulation for treatment-resistant depression. Neuron, 455: 651-60.
31. Polk and Postow (1996) Biological effects of electromagnetic fields. CRC Press, ed. 2. 1996, Boca Raton, FL: C. Polk and E. Postow. 67.
32. Ranck J B, Jr. (1963) Specific impedance of rabbit cerebral cortex. Exp Neurol, 7: 144-52.
33. Sekino M, Inoue Y, and Ueno S (2004) Magnetic resonance imaging of mean values and anisotropy of electrical conductivity in the human brain. Neurol Clin Neurophysiol, 2004: 55.
34. Hemm S, Vayssiere N, Mennessier G et al (2004) Evolution of Brain Impedance in Dystonic Patients Treated by GPi Electrical Stimulation. Neuromodulation, 72: 67-75(9).
35. McIntyre C C, Mori S, Sherman D L et al (2004) Electric field and stimulating influence generated by deep brain stimulation of the subthalamic nucleus. Clin Neurophysiol, 1153: 589-95.
36. Gallay M N, Jeanmonod D, Liu J et al (2008) Human pallidothalamic and cerebellothalamic tracts: anatomical basis for functional stereotactic neurosurgery. Brain Struct Funct.

Tables

Table 1. Electrical conductivity values for different brain matters at 145 Hz [19].

Brain matter	Electrical conductivity (S/m)
CSF	2
Grey matter	0.09
White matter	0.06
Blood	0.7

Table 2. Clinically effective parameter settings.

Electrode	Contact	Electric potential (V)	Pulse width (μs)	Frequency (Hz)
Left	1	-3.5	90	145
Right	7	-3.0	60	145

Figures

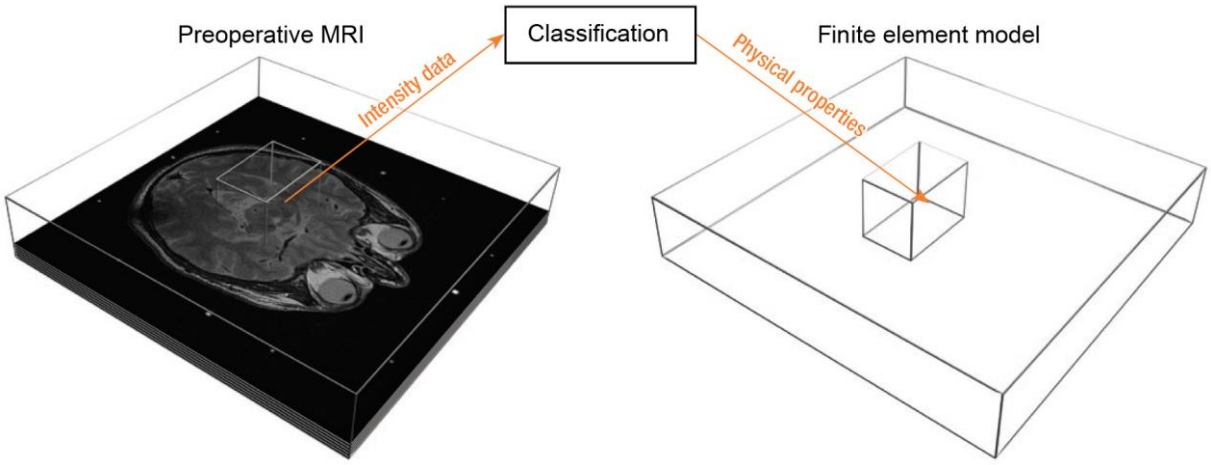

Figure 1. The brain model was set up by extracting preoperative MRI intensity data values which were classified into different material groups such as grey and white matter, cerebrospinal fluid and blood. Each classified MRI intensity data value was allotted its electrical conductivity value and mapped in the finite element model at coordinates corresponding to their original location in the MRI data set. The result was a property matrix of the brain with the same spatial resolution as the MRI data set.

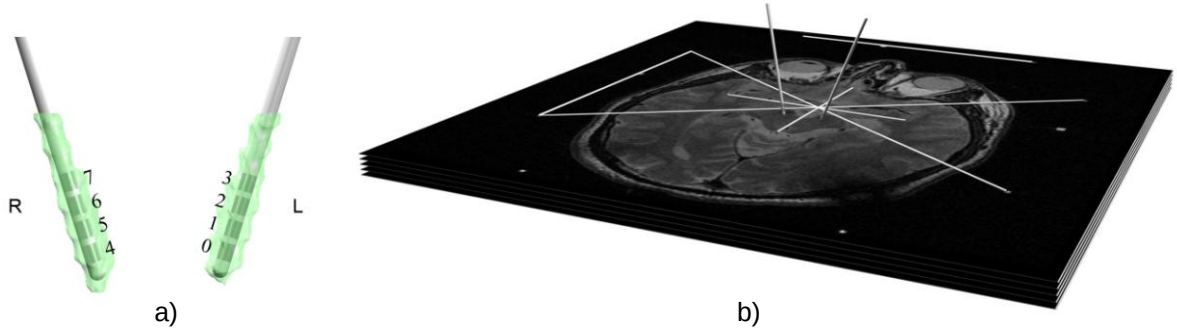

a) b)

Figure 2. a) The electrode contacts were indexed from 0 to 7 starting at the left, most ventral electrode contact. In order to position the DBS electrodes at their true positions, a second brain model based on postoperative MRI was set up. The electrodes were positioned in the centre of the electrode artefacts (green). b) The electrodes were transferred from the postoperative model to the preoperative model by using the markers of the stereotactic localizer box in the MRI together with linear transformation and rotation according to their new coordinate system.

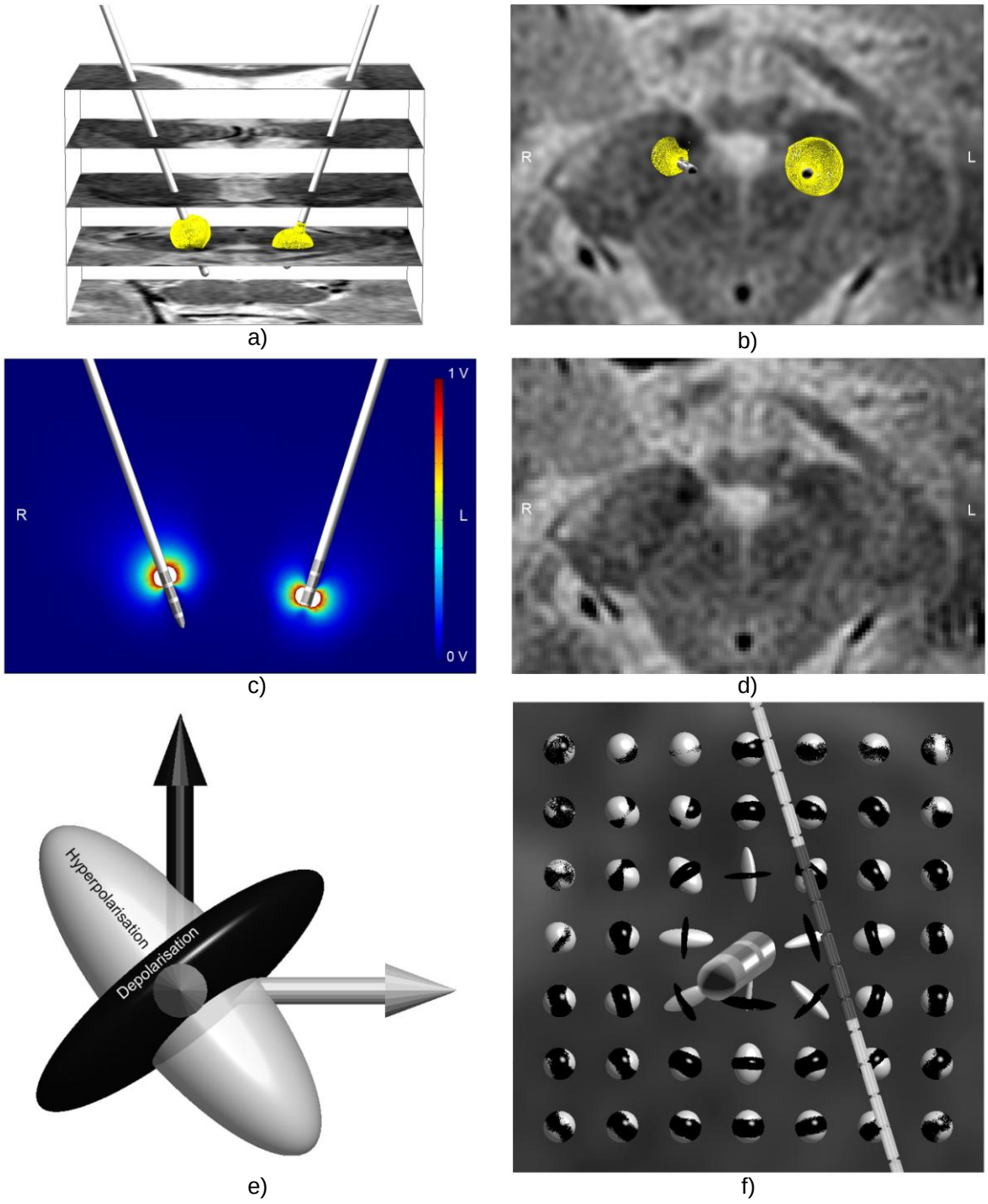

Figure 3. a) Patient-specific simulation of bilateral DBS in the STN during clinically effective stimulation settings. The electric field was visualized with isosurfaces at 0.2 V/mm (yellow). b) Axial model slice visualizing the electric field isolevel at 0.2 V/mm (yellow) together with the anatomy. c) Colour-coded coronal slice visualizing the electric potential in the vicinity of the active electrode contacts. The electric potential was capped at 1 V. d) Axial MRI at the same slice position as the axial model slice in 3b to comparison of the spatial resolution of the model with the MRI data set. e) Two elliptic glyphs illustrating the impact of the electric field on straight axons in one point. The black glyph illustrates the depolarisation effects on straight axons, and the

white glyph illustrates the hyperpolarisation effects of straight axons. f) Axial model slice in the vicinity of the left electrode. The activating function was visualized with a second order tensor field for all direction in 3D. An oversized axon was added to the tensor field in order to display the areas of depolarisation (grey) and hyperpolarisation (white).

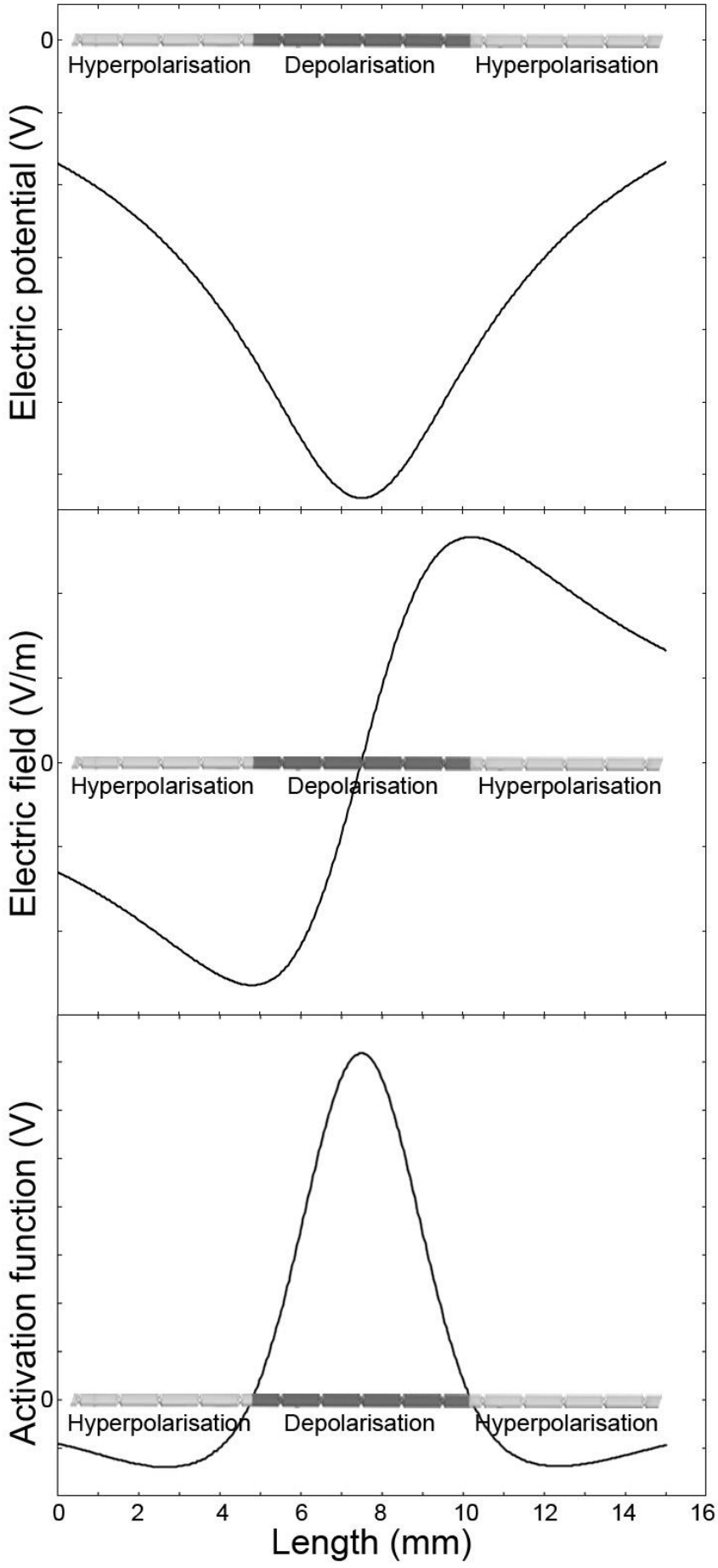
0
Hyperpolarisation
Depolarisation
Hyperpolarisation
Electric potential (V)
Electric field (V/m)
Activation function (V)
0 2 4 6 8 10 12 14 16
Length (mm)

Figure 4. The electric potential, the electric field, and the activating function were visualized with graphs along a straight axon (as illustrated in figure 3f) in the vicinity of the DBS electrode. The axon was added to the graphs in order to visualize areas of depolarisation (grey) and hyperpolarisation (white).

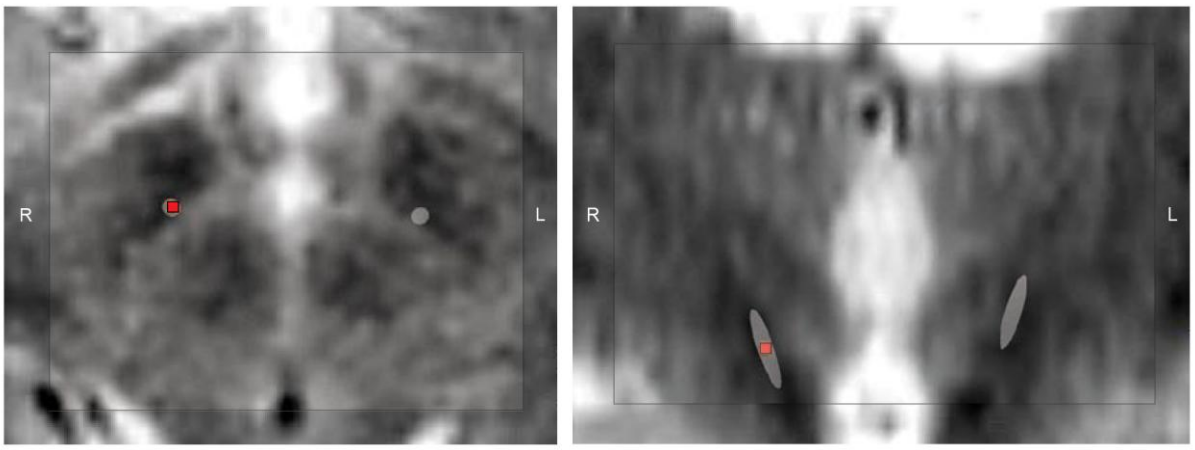

a) b)

Figure 5. The position of the electrode contacts were marked with a red square in the postoperative MRI and transferred to the preoperative MRI using the FrameLink Planning Station™. The positions of the electrode contacts in the model and in the MRI were visually compared by superimposing the images onto each other. a) Two superimposed axial slices at the level of electrode contact 7 for validating the electrode position. b) Two superimposed coronal slices at the level of electrode contact 7 for validating the electrode position.

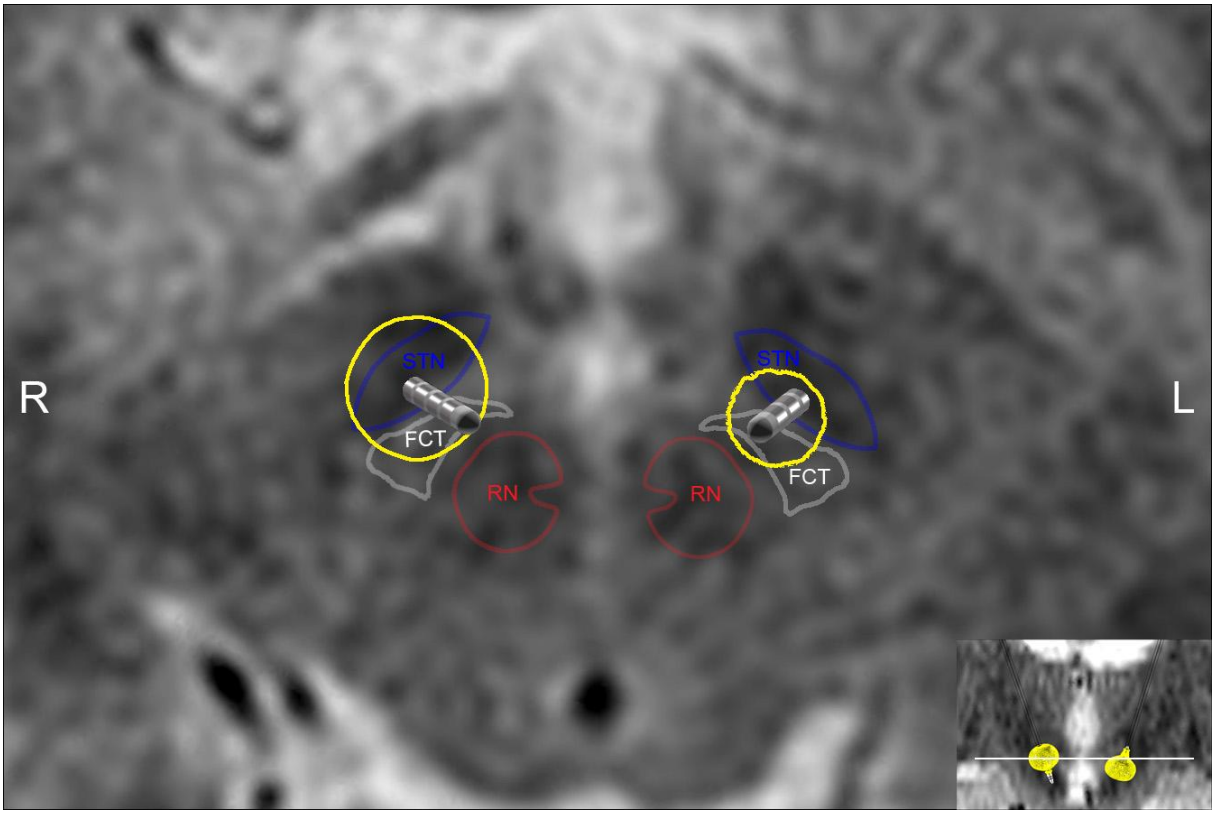

a)

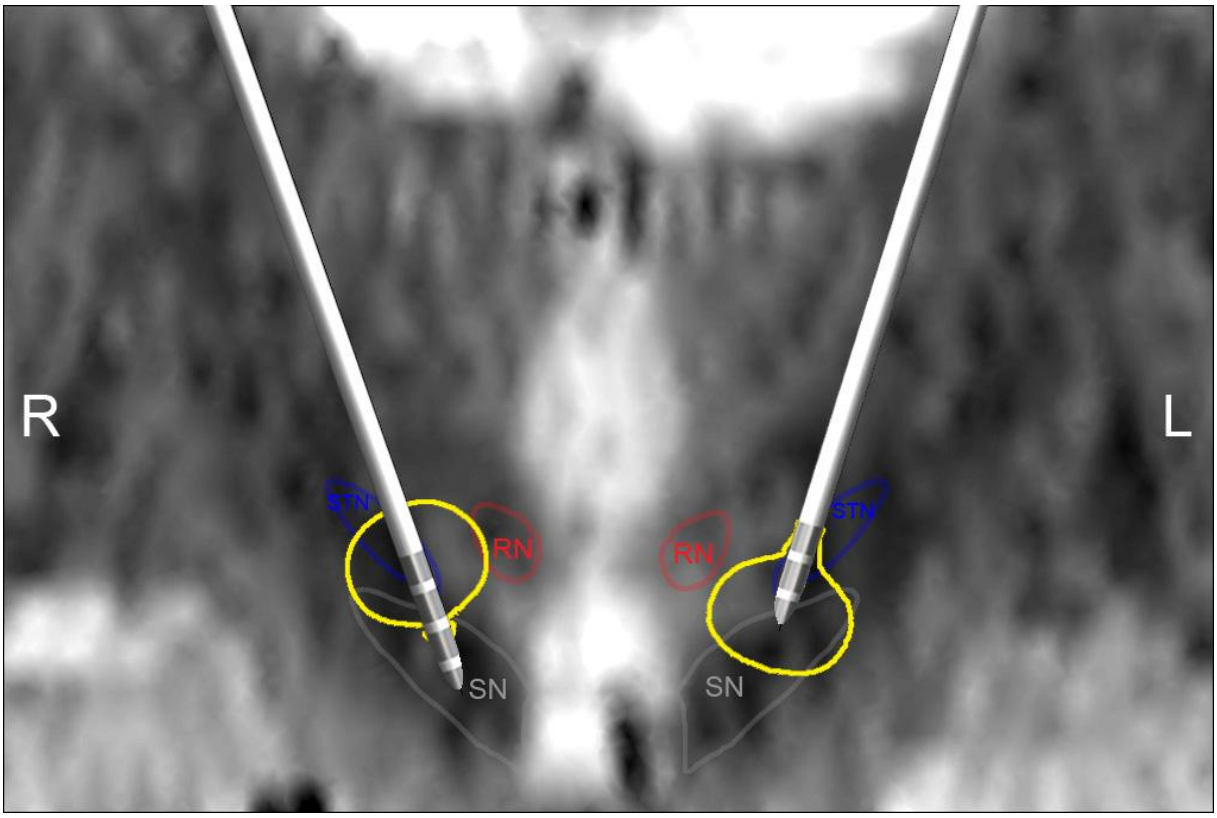

b)

Figure 6. The electric field 0.2 V/mm isolevel was traced onto the axial and coronal images (yellow). Some of the anatomical structures in the vicinity of the electrodes were traced with help of an atlas in Gallay et al. [36]. a) Axial slice showing the electric field isolevel covering part of the fasciculus cerebello-thalamicus (FCT). b)

Coronal slice showing the electric field isolevel generated by the left electrode covering part of the substantia nigra pars reticulata. STN = subthalamic nucleus, FCT = fasciculus cerebello-thalamicus, RN = red nucleus and SN = substantia nigra.